Sphere-Growth Based Centreline Extraction of Murine Airways from Microfocus X-Ray Computer Assisted Tomography

Nicholas Udell[1]
npu1v07@soton.ac.uk
Ian Sinclair[1]
I.Sinclair@soton.ac.uk
Hans Michael Haitchi[2]
H.M.Haitchi@soton.ac.uk
Mark S. Nixon[3]
msn@ecs.soton.ac.uk
Philipp J. Thurner[1]
P.Thurner@soton.ac.uk

[1] Faculty of Engineering and the Environment
University of Southampton
Hampshire, UK

[2] Faculty of Medicine
University of Southampton
Hampshire, UK

[3] Faculty of Physics and Applied Sciences
University of Southampton
Hampshire, UK

Abstract

This paper demonstrates ongoing work on an algorithm for spatially resolved lung morphology assessment of murine lungs, which can also be applied to other 3D branching structures. The algorithm was developed with a view to application on Microfocus Computer Assisted Tomography Data of murine pulmonary structure that has been remodelled due to A Disintegrin And Metalloproteinase (ADAM) 33 gene misexpression, in order to quantify the contributions ADAM 33 misexpression makes towards asthma.

1 Introduction

Microfocus X-Ray Computed Tomography (μCT) is a technique which uses X-Rays to non-destructively image samples in three dimensions, achieving typical spatial resolutions in the order of 1 μm. Resulting raw data sets are large, e.g. a 2000x2000 pixel detector will produce an unoptimized data set of $\sim$32GB at 32 bits dynamic range. The complexity, size and 3D nature of the data make manual extraction and quantification difficult and time consuming, and must consider human error. As such an automated approach, or one that minimizes the time and error cost associated with human involvement, would be a vital tool for pulmonary research.

There are four common methods for analysing the pulmonary branching structure: knowledge based segmentation, region growing/wave propagation, centreline extraction, and mathematical morphology [4]. Typically, solutions in the literature involve a combination of techniques, of which one of the most common is centreline extraction.

Centreline extraction produces a single-voxel wide string representing the central positions of the airways, connecting at branching points. This result reduces the complexity of

the structure to a more easily machine-understood format and allows the user to disassemble the structure into individual branches or generations. The centreline encompasses the length of branches, their orientations and the difference in angles from branches. It is typically found through either tracing or thinning. Unlike thinning, which typically operates equally on all parts of the structure, tracing can handle different cases (e.g. branches versus straight sections). Tracing makes use of a technique for finding the centre of cross sections at successive points along the structure, joining the centres to find the skeleton. Sphere growth is a powerful tool for finding the centre of a cross section of pulmonary structure because the shape will fit well inside any convex shape and the growth of the sphere is robust against surface noise. Additionally it can be used to find the orientation of the structure it has been grown in for better-informed positioning of the next cross section, and a rudimentary measure of airway radius can be obtained by taking the radius of the fully-grown sphere.

Swift *et al*. [5] and Carrillo *et al*. [1] use spheres to trace the skeleton of the pulmonary tree, but in different ways. Swift *et al*. use tessellated spheres to find patches of air 'in front' of the tracer's current position. This is deemed to be a 'future point' or next step along the airway. If multiple patches are found, these are considered to be branches. Centreline positioning is found using a separate step, which uses 2D ray-casting to find contours in an oblique slice. Carrillo *et al*. use inflated spheres combined with connected components analysis to find centreline positioning. An initial guess for centreline position is obtained, and a sphere grown around the point. The first intersection between airway wall and sphere is recorded and the sphere is grown until another intersection is recorded along the vector from the first towards the sphere centre. The difference in sphere radii for first and last contacts is used to move the centre point (and sphere) along the vector. Future points are detected by extending the sphere once growth is complete and detecting connected components which are inside the extended sphere and are left when the original sphere is subtracted. Similarly to Swift *et al*., branch points are detected by finding multiple connected components.

This paper proposes a modified version of Carrillo *et al*. that corrects centreline position using sphere inflation with multiple intersection sources. Instead of using connected components analysis, it calculates future trace points using plane-fitting to find the orientation of the airway cross-section and detects branch points using radial ray casting.

2 Methods

Wild-type mice were terminally anaesthetised and their lungs inflated with Microfil (Flow Tech, Inc.) at a constant rate of 10μl per second to a constant total volume. Once the required volume had been injected, the trachea was tied off and the lung removed from the chest and placed in 4% Paraformaldehyde and stored at 4C. The next day, the lung was transferred to a vial filled with PBS plus 6% sucrose and stored at 4C.

To keep the samples in a stable position they were transferred to 15mm Bijoux tubes filled with a 30% solution of Lutrol F68 (BASF Chemicals) and brought to room temperature, where the F68 gel thickened. The lungs were then imaged in batch in custom 225kV Nikon/Metris HMX ST scanner (HMX) at 115Kev and 85mA. Images were converted to 8 bit brightness range and cropped to remove surrounding void, before being filtered with a 3x3 median filter and binarised using a uniform threshold set to the highest intensity peak in the intensity histogram. The binarised image was eroded and then dilated to remove any small structures or noise which connected structures erroneously.

The images were processed using a tracing algorithm implemented in MATLAB, which

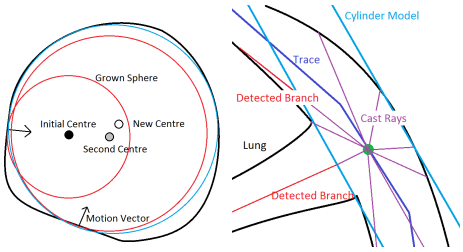

Figure 1: Left: Diagram showing initial sphere inflation, and motion vectors successively correcting the sphere centre position. Right: Diagram showing branch detection by ray casting. Rays that pass through the cylindrical model built around the ray's origin are considered branches.

takes a manually-entered seed point and makes informed positional jumps through the airways. At each jump, the centre of the cross-section of the airway is extracted and the airway's orientation calculated. This information is used to find the coordinates of the next point using equation (1).

$$C_{n+1} = C_n + \hat{\mathbf{o}}_n(r_n\alpha) \tag{1}$$

where C is the position of the tracer in the image, $\hat{o}$ is the orientation vector, r is the radius of the cross section of the structure found at coordinate C, using equation (3) and α is a pre-supplied accuracy factor for speed/accuracy trade-off.

After each jump, we use a sphere-growth algorithm (equation (2)) to find the cross-sectional centre to find the maximally enclosed sphere within the structure.

$$\gamma_{n+1} = \gamma_n + \hat{\mathbf{m}} \tag{2}$$

where γ is the centre of the current sphere and $\gamma_0 = C_n$ from (1) and $\mathbf{m}$ is the direction vector in which to move the centre point and is defined as:

$$\mathbf{m} = \delta - \frac{(\delta \cdot \hat{\mathbf{o}}_n)}{\|\hat{\mathbf{o}}_n\|^2}\hat{\mathbf{o}}_n \tag{3}$$

where $\mathbf{o}$ is from equation (1) and δ is defined as:

$$\delta = \sum_{i,j,k=0}^{n} (f(r,C_n)_{ijk} \cap D_{ijk})[i - C_{ni}, j - C_{nj}, k - C_{nk}] \tag{4}$$

where $f(r,C_n)$ is a function which finds the set of points on the circumference of the sphere with radius r and centre C_n, $D_i jk$ is the value of point (i,j,k) in the lung data set and where r is the maximal radius of a sphere centred at (i,j,k) within the structure.

After each growth pass, we sum vectors pointing from sphere-airway intersections towards the sphere's centre to create a vector pointing away from the walls (equation (4)) for as long as it can continue expanding. Figure 1 shows a diagram of this part of the algorithm in action. The sphere's motion is restricted to be along the plane normal to the previous orientation estimate to prevent it moving through the airway. Airway orientation is found by plane fitting to the set of structure/sphere intersections on the final inflated sphere, and taking the normal of this plane.

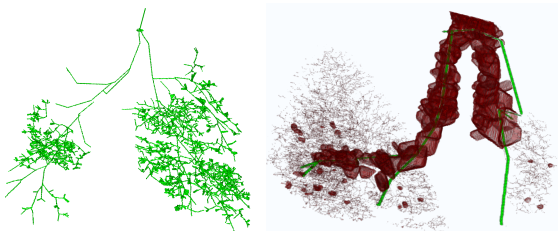

Figure 2: Left: Trace of a murine wild-type lung. Right: Close up of the primary branch of the same trace (green) compared with the result of the binary thinning skeletonization algorithm in the Fiji ImageJ Package (http://fiji.sc), based on [2] (dark red)

Airway branches are found by casting rays from each voxel between jump points in the trace. The distance between the trace position and the closest intersection of ray and airway is divided by an expected value as shown in equation (5), which is calculated from a cylindrical model $\frac{r}{\sin(\arccos(\hat{\mathbf{o}}\cdot\hat{\mathbf{d}}))}$. See figure 1 for a diagram of this process.

$$b_r = \frac{f(\gamma_n, \hat{\mathbf{d}})\sin(\arccos(\hat{\mathbf{o}}\cdot\hat{\mathbf{d}}))}{r} \tag{5}$$

where γ_n is defined in (2), d is the direction of the ray being cast, r is the radius of the airway found during previous sphere inflation, $f(\gamma_n, \hat{\mathbf{d}})$ is a function that is defined in equation (6) that finds the distance between γ_n and the closest airway wall point along the line defined by direction vector $\hat{\mathbf{d}}$.

$$f(\gamma_n, \hat{\mathbf{y}}) = \min_{p\in\mathfrak{N}, p>0} \begin{cases} \|\hat{\mathbf{y}}_p\|, & d(\gamma_n + \hat{\mathbf{y}}_p) \geq 1 \\ \infty, & \text{otherwise.} \end{cases} \tag{6}$$

where $d(x)$ is a function that finds the value of the binarised image at position x.

Any values for b_r which are greater than 2.5 are considered potential branch indicators. These are sorted by b_r and the most likely branch traced first. Due to the number of branch detection measurements taken it is likely that the same branch is detected multiple times at different jump points along the trace. In order to prevent false positives, all traced data are removed from the working image. Any branch coordinate that is in void is discarded as a duplicate when loaded to be traced. This also has the effect of removing erroneous branches detected due to airway curvature being mistaken as a branch (see figure 1 for an example).

3 Results

In order to prevent excessive false positives, the tracer was instructed to stop at any structure with radius less than 8 voxels, so some airways after the 4th generation have been missed. The traces (see figures 2 and 3) were computed in 5 hours each on a single core of an Intel Core i7 2.8GHz CPU (Intel Corporation, California) computer with 16GB of RAM.

Validation of the algorithm was performed by tracing with multiple seed points offset from a base, user-picked seed. The resultant traces were compared with each other by finding, for each branch point in a trace, the geometrically nearest branch point in the other traces

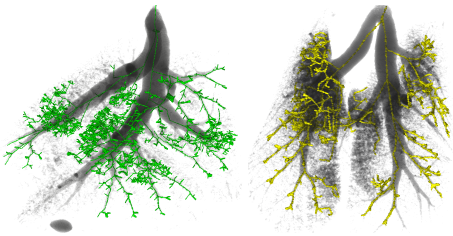

Figure 3: Two different wild-type lungs (grey) with their traces superimposed.

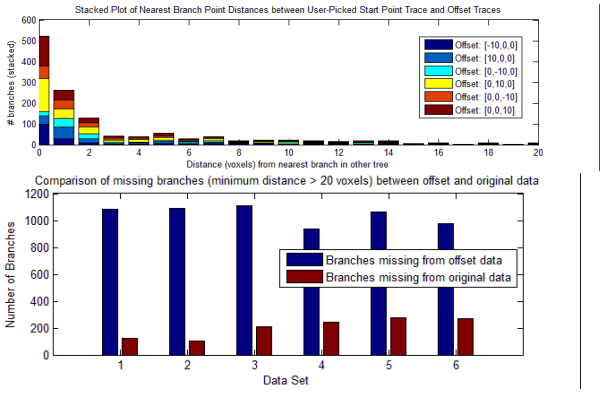

Figure 4: Top: Histogram showing range of branch point distances over 6 offset seed positions from a user-picked seed point. Bottom: Bar chart showing number of unregistered branches for the seed points used.

(see figure 4). This system was also able to highlight branches which were found in some systems but not in others.

4 Discussion

The skeleton produced by the algorithm is cleaner and more intuitive than the binary thinning algorithm's results. The tracer returns a single connected string of voxels denoting the branching structure's centre, the thinning algorithm returns a set of 3D faces and shows less noise tolerance. With the tracer, branches are detected and stored on the fly, and during thinning, branch detection must be performed as a post-process. Also it is difficult to incorporate prior knowledge (such as branching statistics) into a thinning-based algorithm as it operates indiscriminately across the entire dataset, whereas the tracing system possesses knowledge of the overall branching structure as it executes. This allows applications to sacrifice a generalised algorithm for accuracy or speed or to remove the manual step.

The high values for branches missing from offset data in figure 4 is due to the offset traces having missed the primary airway branch point. The seed point was too close to the branch due to model limitations, and the offset exacerbated difficulties with branch detection. As such half of the airway tree to be missed, however this can be fixed by beginning an

additional trace in the remaining data and joining the two trees. Additionally, some missed branches can be caused by the tracer entering areas of insufficient contrast such that noise and airway become indistinguishable. This leads to a knot of erroneous branches which can be seen in figures 2 and 3. It is important to note that when the same branches are found, their positioning is very consistent, as can be seen in figure 4.

On the other hand, the thinning algorithm guarantees to skeletonize the entire structure, including disconnected segments and difficult to analyse branches. The thinning algorithm is also faster, taking 3 hours to compute on the same machine, however it is possible it was multi-threaded. Finally, it requires no parameters to execute consistently, whereas the tracer uses a seed point and an accuracy factor to be input at the beginning of execution, after which it can be left unattended until it is finished. It is possible to automate the seed point discovery by searching for the largest branch, however this would limit the algorithm's application in relation to non pulmonary systems which may have different layouts.

5 Conclusion

The clear advantages inherent to the tracer are its cleaner, single line result, which allows the user to collect measurements consistently from each branch. The fact that the tracer builds the tree with prior knowledge from the root of the branching structure allows the tree to be labelled and measurements extracted and compared on a per-generation basis. Additionally, the tracer inherently incorporates connected components and will only extract tube-shaped structures, ignoring any connected masses.

Importantly, we demonstrate an algorithm for spatially resolved lung morphology assessment of murine lungs. After further validation we will apply this algorithm to assess changes in lung morphology due to over-expression of ADAM33. This algorithm will offer not only a tool to assess airway remodelling in small animal models of airway inflammation and remodelling as well as in human lung disease, but also a tool which can measure structural parameters in other branching structures, such as plant roots, kidney vasculature, etc.

References

[1] Carrillo et al. Extraction of 3d vascular tree skeletons based on the analysis of connected components evolution. In *Computer Analysis of Images and Patterns*, pages 604–611. Springer, 2005.

[2] Lee et al. Building skeleton models via 3-d medial surface/axis thinning algorithms. *CVGIP: Graphical Model and Image Processing*, 56(6):462–478, 1994.

[3] Masoli et al. The global burden of asthma: executive summary of the gina dissemination committee report. *Allergy*, 59(5):469–478, 2004.

[4] Sluimer et al. Computer analysis of computed tomography scans of the lung: a survey. *Medical Imaging, IEEE Transactions on*, 25(4):385–405, 2006.

[5] Swift et al. Automatic axis generation for virtual bronchoscopic assessment of major airway obstructions. *Computerized Medical Imaging and Graphics*, 26(2):103–118, 2002.

[6] Van Eerdewegh et al. Association of the adam33 gene with asthma and bronchial hyperresponsiveness. *Nature*, 418(6896):426–430, 2002.